November 2000 • NREL/MP-570-29069

Milestone Report

Laminar Entrained Flow Reactor for Biomass Thermochemical Conversion Studies

Milestone Completion Report

D.C. Dayton

For the Chemistry of BioEnergy Systems Center

National Renewable Energy Laboratory

1617 Cole Boulevard
Golden, Colorado 80401-3393

NREL is a U.S. Department of Energy Laboratory
Operated by Midwest Research Institute • Battelle • Bechtel

Contract No. DE-AC36-99-GO10337

NOTICE

Available electronically at http://www.doe.gov/bridge

Available for a processing fee to U.S. Department of Energy
and its contractors, in paper, from:

U.S. Department of Energy
Office of Scientific and Technical Information
P.O. Box 62
Oak Ridge, TN 37831-0062
phone: 865.576.8401
fax: 865.576.5728
email: reports@adonis.osti.gov

Available for sale to the public, in paper, from:

U.S. Department of Commerce
National Technical Information Service
5285 Port Royal Road
Springfield, VA 22161
phone: 800.553.6847
fax: 703.605.6900
email: orders@ntis.fedworld.gov
online ordering: http://www.ntis.gov/ordering.htm

Printed on paper containing at least 50% wastepaper, including 20% postconsumer waste

Milestone Completion Report:
Laminar Entrained Flow Reactor for
Biomass Thermochemical Conversion Studies

Program:	Biomass Power Program
Technology Manager:	Kevin Craig
Milestone Title:	Development of a Laminar Entrained Flow Reactor for Biomass Thermochemical Conversion Studies
Milestone Type:	C, FY00
Completion Date:	6/00
Reported by:	David C. Dayton
Participating Milestone Researchers:	Alexander Brown, Daniel Carpenter
Project:	Ash Deposition/Cofiring Studies

EXECUTIVE SUMMARY

The U.S. Department of Energy's Biomass Power Program is supporting efforts to generate clean electricity from biomass. Technologies range from traditional direct combustion systems to raise steam to advanced integrated gasification combined cycle systems with high projected efficiencies. The initial step in all biomass thermal conversion systems is the initial pyrolysis of the solid feedstock. A reliable description of the global kinetics of biomass pyrolysis is the building block for accurately describing the high temperature chemistry that occurs in developing biomass thermochemical conversion systems. These accurate chemical models of biomass gasification and combustion can be used as input in systems analysis models to adjust engineering parameters such as gas velocities, particle residence times and heat transfer rates to optimize the design and performance of developing technologies.

To address the need for accurate chemical kinetic measurements of biomass thermal conversion, a new laminar entrained flow reactor (LEFR) is being designed, fabricated, and characterized for studying biomass pyrolysis and gasification kinetics. Biomass will be continuously fed into the reactor and product gases will be monitored with a molecular beam mass spectrometer system. This new experimental technique will be complimentary to previous biomass combustion, gasification, and pyrolysis studies that used batch sample introduction. The batch aspect of the previous experiments, however, made it difficult to extrapolate results to large-scale biomass conversion systems. The development of the LEFR is expected to facilitate the extrapolation of results obtained from bench-scale experiments to larger scale systems.

The newly designed, continuously fed, bench-scale, entrained-flow reactor will be used to determine the rates of evolution of pyrolysis products, gasifier tars, and ultimately alkali metals. If the reactor is operated under laminar flow conditions it will be possible to accurately model the reactor using existing computational fluid dynamics computer codes. These models will facilitate the interpolation of the batch combustion results to continuous-feed experiments and the extrapolation of the bench-scale-derived information to larger scale biomass combustors and gasifiers. The ultimate goal of modeling in the bench-scale experiments is to determine whether we can take results from the simplest batch combustion experiments and extrapolate to commercial-scale.

Much of the work that has gone into the design and characterization of the new LEFR indicates that particle pyrolysis can be accurately controlled in this reactor. A combination of measurements and theoretical modeling contribute to a detailed understanding of the operating qualities of the reactor. Excellent agreement exists between the model and the measurements when overlapping data exist between the two analytical techniques. Maintaining kinetic, rather than heat transport control is important to experimental value. Maintaining small (<50 μm) particle sizes is critical to both the control regime and to particle velocity lag in the reactor.

Table of Contents

LIST OF FIGURES

INTRODUCTION

A newly designed instrument has been characterized for use in studying biomass pyrolysis processes. It is a laminar entrained flow reactor (LEFR), also commonly known as a drop-tube reactor. It is essentially a vertical quartz tube. Particles are introduced at the top of the reactor and they drop into a laminar gas flow. The injection tube can be moved, thus adjusting the height at which particles are exposed to the high temperature regions of the reactor. Particles react according to the temperature of the reactor, which can be controlled by a four-zone ceramic furnace. This particular reactor was designed with a horizontal sampling tube. Through this tube, gas phase species emitted from the solid material are sampled. A 90-degree conical section at the end of the sampling tube connects the reactor with a molecular beam mass spectrometer (MBMS), which is used to analyze the gas phase species emitted from the high-temperature region of the reactor.

This type of reactor is not unique. Such reactors have been used extensively, and there is good information on the design, characterization, and uses of this type of an instrument. LEFRs have been used extensively to study particulate pyrolysis, and documents that address characterization and theory of operation are abundant in the literature [Fletcher, 1989; Fletcher, 1993; Jamaluddin, et al., 1986; Pollard, 1997; Wagenaar and Van Den Heuvel, 1997; Westerhout et al., 1996]. LEFRs are generally used to control solid heating rates and collect the residual solid mass for analysis. We hope to apply this technology in a different manner, by sampling and measuring the high-temperature gas phase products with our MBMS systems. The reactor should allow us to accurately control the pyrolysis history of the particles, and thus examine various pyrolysis regimes that are otherwise obscured by transport and signal limitations. Understanding the operation dynamics of this instrument will be critical to the goals of this study. This report presents the results of the design and characterization of the LEFR.

THE REACTOR

Traditionally, batch type reactors have been used with an MBMS to study biomass [Dayton, Belle-Oudry, and Nordin, 1999; Dayton, et al., 1999; Dayton and Milne, 1996; Dayton, French, and Milne, 1995; Evans and Milne, 1987a,b]. Typically samples on the order of 20 mg are placed in a quartz boat and inserted into the hot zone of the reactor. An inert gas flows through the reactor, and product gases are monitored. A typical pyrolysis event lasts from a few seconds to about one minute. Heating rates are approximately 10-100 K/s.

Batch reactors can be used to monitor product formation as a function of temperature and fuel type. Kinetic rates and devolatilization regimes are difficult to analyze with this technique, as heat transfer within the sample tends to obscure the data. Another common technique for studying devolatilization kinetics is thermo-gravimetric analysis (TGA) [Orafao, 1999; Lanzetta and Di Blasi, 1998; Koufopanos, et al., 1991 and 1989; Ward and Braslaw, 1985]. This involves weighing a sample as it is heated in a carefully controlled environment. Such experiments typically involve small samples, with an upper limit being of about 20 mg. Larger samples require lower heating rates to maintain reaction control. The heating rates are typically approximately 1-100 K/min. Again, mass loss occurs in an inert gaseous environment. The low heating rates, small sample size, and controlled temperatures allow for accurate rate determination. These characteristics also inhibit the ability to accurately sample and analyze the product gases, as the products tend to be in low concentrations relative to the bulk gas flow. Furthermore, industrial processes typically involve much higher heating rates. Data extrapolation is necessary when applying TGA results to most practical systems.

A properly characterized LEFR is capable of circumventing many of the limitations of the more classical analytical techniques. A major advantage is that samples are introduced into the reactor as individual

particles rather than bulk samples. Thus, heat and mass transport limitations are minimized, permitting much higher heating rates while maintaining reaction control. Increasing the inlet flow rate of the bulk material may augment product concentrations. When all particles undergo similar time-temperature histories, products from various devolatilization regimes may be more closely and accurately examined.

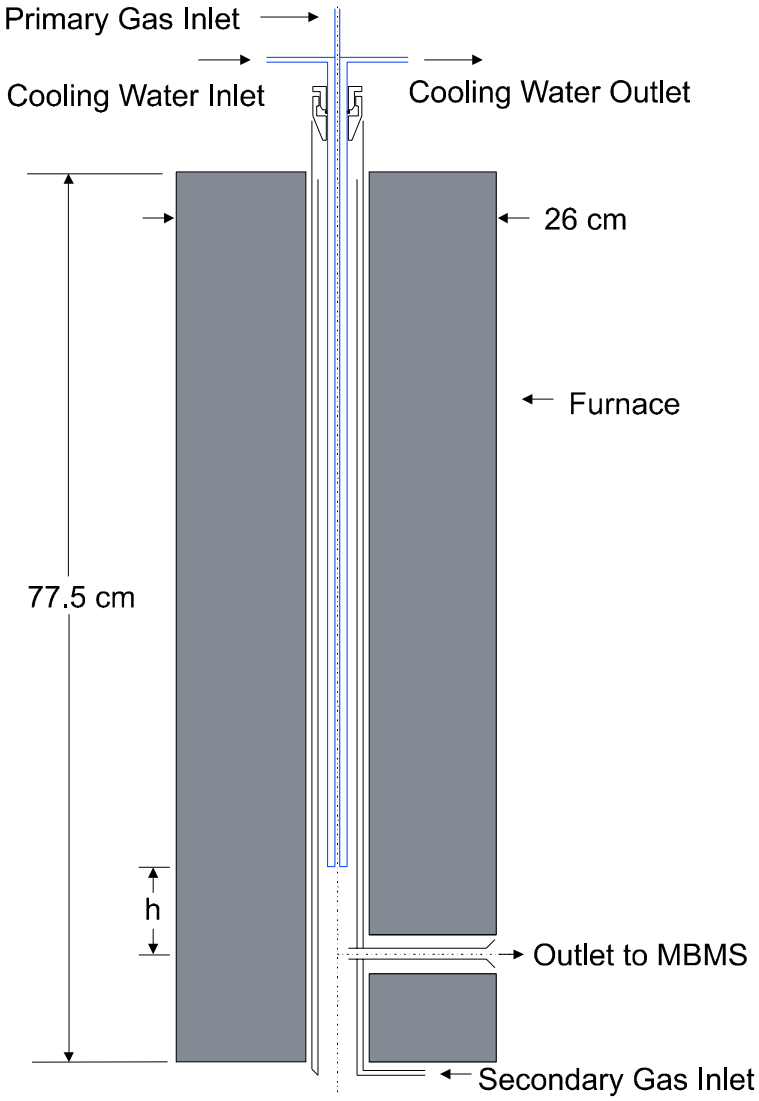

Figure 1: An illustration of the LEFR

Figure 1 is an illustration of the LEFR. The primary gas stream with entrained particles flows down the centerline of a 0.435 cm i.d. water cooled quartz feeder tube. An o-ring and threaded sealing plug is used to adjust the height of the feeder tube in the reactor and create a gas tight seal between the tube and reactor. The feeder tube is approximately 83 cm total in length. The reactor consists of two concentric tubes, one a 4.1-cm o.d., and the other a 3.2-cm o.d. Secondary gas flows into the bottom of the outer flow region, and heats up as it flows up between the two quartz walls. At the top of the reactor, the gas reverses direction and flows down the center flow region, where the inner reactor tube and the outside of the water-cooled feeder tube are the boundary walls. At about 9 cm from the bottom of the reactor, a 1.0-cm o.d., 0.585-cm i.d. quartz sample tube penetrates into the flow region. Gas flows down this tube to a

90-degree cone at the end of tube, where the 90-degree inlet skimmer to the MBMS system is placed to sample the reaction products. A small 0.1-cm i.d. tube runs lengthwise along the inner quartz reactor tube from the bottom of the reactor up the length. A small thermocouple is slid up the tube wall to accurately measure the wall temperature. The reactor is placed inside a 26-cm diameter, 77.5-cm high four-zone electrically heated ceramic furnace. Primary gas flows are between 100 and 500 sccm of helium, and secondary gas flows are between 1 and 3 slm of helium. In cold flow experiments, cellulose particles were injected down the centerline feeder tube. Flow was observed to be laminar for the indicated flow rate conditions, as the cellulose particles traced a smooth line from the feeder tube outlet to the bottom of the reactor. Calculations also yield low values for the Reynolds number in all tubular sections of the reactor, further indicating laminar conditions. As particles exit the feeder tube into the reactor region, they are rapidly heated to the same temperature as the external wall. Peak heating rates are estimated to be on the order of 10^4 K/s, and particle residence times are typically about 1 s.

CHARACTERIZATION

The time-temperature history of a particle in the LEFR is the primary focus of all characterization, as this relationship can, in theory, determine the extent to which the solid material reacts. This is a complex process. The local gas temperature is a function of the furnace settings, heat transfer in the reactor, and fluid mixing processes. Particle temperatures are influenced by radiative and convective transport, internal conduction, chemical reactions, and perhaps by wall impact. Particle residence times are a function of the local gas flow rate, which is a function of temperature through the ideal gas relationship. Times also depend on the path the particle takes. This depends on particle density, gravity, size, heat capacity, and to some degree on particle starting location. Clearly, a simple model is not sufficient to illustrate the complexity of this problem, particularly the transition flow regions as the primary and secondary gases mix, and the 90-degree turn region of the reactor. Computational fluid dynamics (CFD) simulations are employed to model many of these complex processes, as the geometry and input conditions can be accurately measured. CFD can then output a time-temperature profile for a particle, and the data then can be checked against measured quantities.

The following sections discuss characterization results and provide a glimpse of the type of information that will be measurable with the current reactor design.

CFD Simulations

Fluent Inc. software version 5 was used to model the transport phenomena within the reactor. Laminar flow facilitates the modeling, as inaccuracies in the turbulence models typically limit CFD accuracy in most cases. Grid design is an another important aspect affecting the accuracy of CFD modeling. A danger with CFD modeling is over-simplifying the grid. This is prevented by incrementally refining the grid and comparing the results to those of the coarser grid. Adequate grid independence has been achieved with a grid made from a mixture of about 60,000 rectangular and tetrahedral cells. Standard convergence criteria are lowered, and convergence is assumed when all continuum residual values no longer change after subsequent iterations.

Gas Temperature

In early CFD models of the reactor, the counter-flow (upward) region of the gas flow was modeled. It was observed that the gas rapidly assumed the estimated wall temperatures in most regions of flow. This means that the outer counter-flow region of the model was unnecessary. It also means that an accurate measure of the inner wall temperatures is critical to determining the gas temperature. The cooling water holds the water-cooled probe to a relatively constant temperature. The inner reactor wall temperatures, however, are a function of internal heat transfer processes.

In order to assess the impact of radiative heat transfer on this problem, a spectral model of heat transport was generated from the Planck distribution:

$$E_{b\lambda} = \frac{C_1 \lambda^{-5}}{e^{C_2/\lambda T} - 1}$$

From transmittance charts, it was observed that quartz is quite opaque in the infrared (IR) region from about 4000 nm and up. The region from 2000 to 4000 nm is a transition region of partial transmittance and below 2000 nm quartz is quite transparent. Integrating the Planck function over these spectral regions calculates the energy of the blackbody spectrum at a given temperature in that spectral region. Figure 2 shows a plot of the radiative energy fraction in each spectral region. Biomass pyrolysis in the reactor occurs from about 350°C to 650°C. It can be seen that the quartz walls are fairly opaque to the bulk of the thermal radiative emissions in the temperature regions of interest. The expected transmissivity in the range of temperatures for this reactor is probably around 10-30% of the bulk energy. Therefore, radiation is likely to contribute little to the heat transfer in the reactor and will not be considered further. Heat transfer in the LEFR will be modeled using conduction and convection.

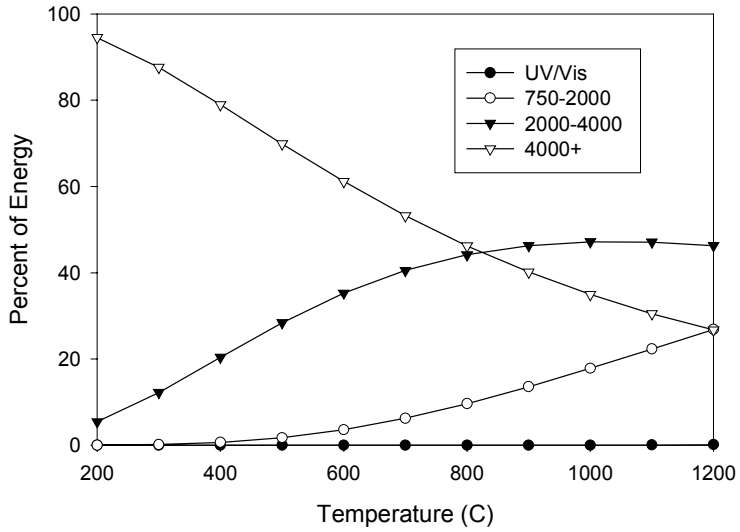

Figure 2: A plot of the blackbody radiative emission fraction for various spectral regimes.

The reactor was subsequently redesigned with a tiny quartz thermocouple well, which progresses up the internal wall of the reactor. Wall temperatures are measured as a function of height. The location of the water-cooled probe was found to significantly impact the wall temperature measurements. Temperatures near the center of the furnace tend to be higher than at the extremities. Gas temperatures were measured by inserting a thermocouple up the centerline of the reactor. Centerline gas temperature measurements were compared to CFD predictions of the centerline gas temperature by using the measured wall temperature profile as an input parameter. Figure 3 illustrates the remarkable agreement between the predicted and measured centerline gas temperatures. Centerline measurements were difficult to make, as the positioning of the thermocouple along the centerline was difficult to maintain precisely. This difficulty is reflected in the slight disagreement in the region of highest temperature gradient between 15 and 20 cm height. Through repetition, it was found that the wall temperature could be accurately

measured to ±2 degrees. Most of this error can be attributed to the cycling of the temperature controllers and inaccuracies in the positioning of the thermocouple. It is therefore expected that inputting the appropriate boundary conditions into the CFD model will result in an accurate prediction of the gas temperature. Initially, comprehensive wall measurements were taken. There is a linear relationship between the temperature of the walls and the temperature setting on the controllers, so subsequent profiles were obtained by interpolating across detailed measurements taken at the temperature extremes.

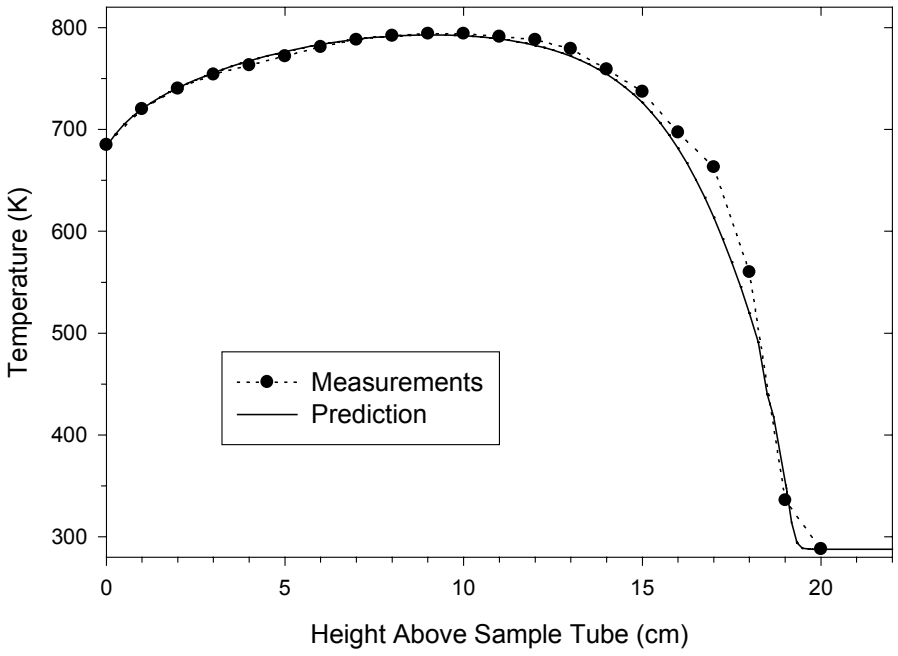

Figure 3: A plot of predicted and measured centerline gas temperatures in the LEFR.

Gas Velocity

The gas velocity is nearly impossible to measure under reactor conditions. Optical access is not available, and positioning physical probes would be difficult. Temperature effects would complicate any measurements. In cylindrical sections of the reactor, plug flow conditions are expected to dominate. Although characterization of these regions would be simple, transition regions would be nearly impossible to predict accurately with a simple correlation or model. Due to these complexities, it is necessary to rely on the CFD simulations to accurately model the gas velocity and trust that adequate system validation is sufficient to validate this assumption.

System Validation

To validate the system, a gas compound with known decomposition rates was chosen. The rate of thermal decomposition for allyl ethyl ether ($C_5H_{10}O$) has been accurately measured [Egger and Vitins, 1974], and the decomposition region is in a similar thermal region as biomass decomposition. The mass spectrum of allyl ethyl ether as observed with a photo-ionization (118 nm) time-of-flight mass spectrometer was measured for furnace temperatures ranging from 380°C to 620°C. The corresponding wall temperatures were also measured. Mass peak signals at m/z=58,86 were integrated and summed to represent the reactant and the mass peak signals at m/z=42,44 were integrated and averaged to represent the product. Figure 4 illustrates a typical mass spectrum of the compound with the furnace temperature

controllers set to 500°C. Data reduction was complicated because of some irregularities in the mass spectrum. The first is the unusual broad signal labeled with a question mark in Figure 4 in the mid to low m/z=50's region. This signal was repeatable, and scaled with the magnitude of the m/z=58,86 peaks. The second was the width of the m/z=58 peak, which extended from just below m/z=58 (typical) to m/z=58.8. We suspect that both are due to molecular decomposition in the drift region or in the reflectron [Neusser, and Krause, 1993]. If this were the case, multiple ions would exist where one was present, and relatively equal non-integer signals would be expected both before and after the true parent peak. Based on this assumption, it is expected that integrating the entire m/z=58 peak and ignoring the mid-m/z=50's signal would produce a representative signal value. The ratio of the product to the total signal gives an estimate of thermal conversion. This is compared to the predicted conversion based on the CFD generated time-temperature profiles and the rate information from the literature.

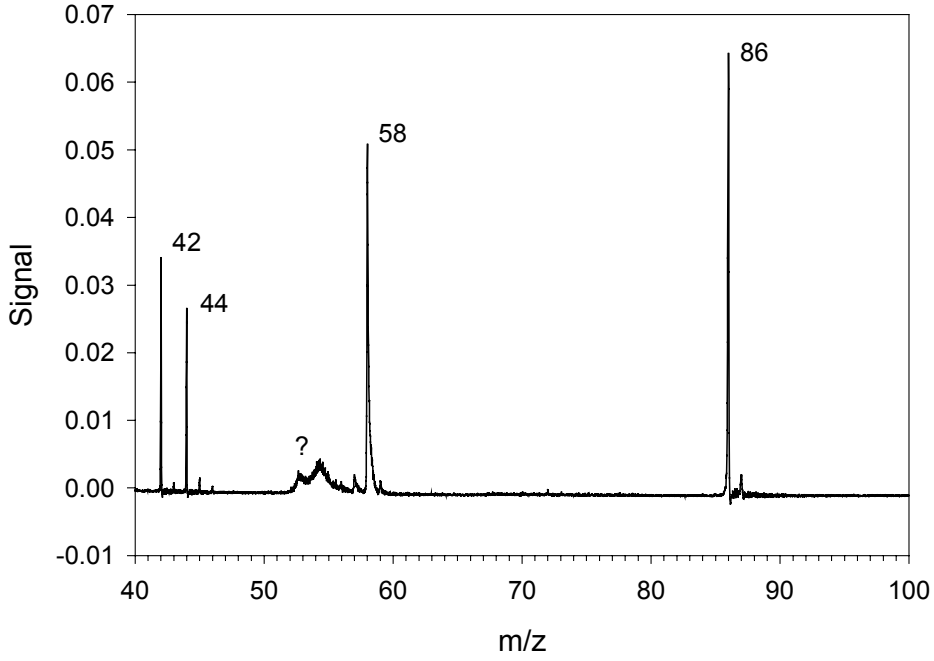

Figure 4: A typical mass spectrum of allyl ethyl ether thermally decomposing in helium at 500°C.

Figure 5 compares the measured and predicted thermal conversion of allyl ethyl ether in the LEFR with the feeding tube at two heights and different gas flow rates. Two additional lines are plotted. One, labeled 'peak magnitudes' is an upper estimate of the conversion from the data based on the magnitude of the mass peaks rather than on the mass peak integral. Since the higher m/z peaks are broader than the lower ones, this analysis technique shows the upper limit of the estimated conversion. The other line labeled 'including noise' is based on the signal in the mid-m/z=50's region being included with m/z=58,86 as reactant signal. Since dissociation is expected to yield multiple ions for one parent, this is expected to give a lower limit of the estimated conversion. The "measured" and "predicted" values for both test conditions match well. These accurate results are particularly encouraging, since the MBMS technique is only considered semi-quantitative due to the variation in ionization cross-sections of the different chemicals. Monitoring of multiple peaks should dampen out the errors caused by the variation in ionization cross-sections. This implies that it may be possible to measure accurate quantitative rate information using the LEFR and MBMS for chemical processes that can be monitored by multiple mass peaks.

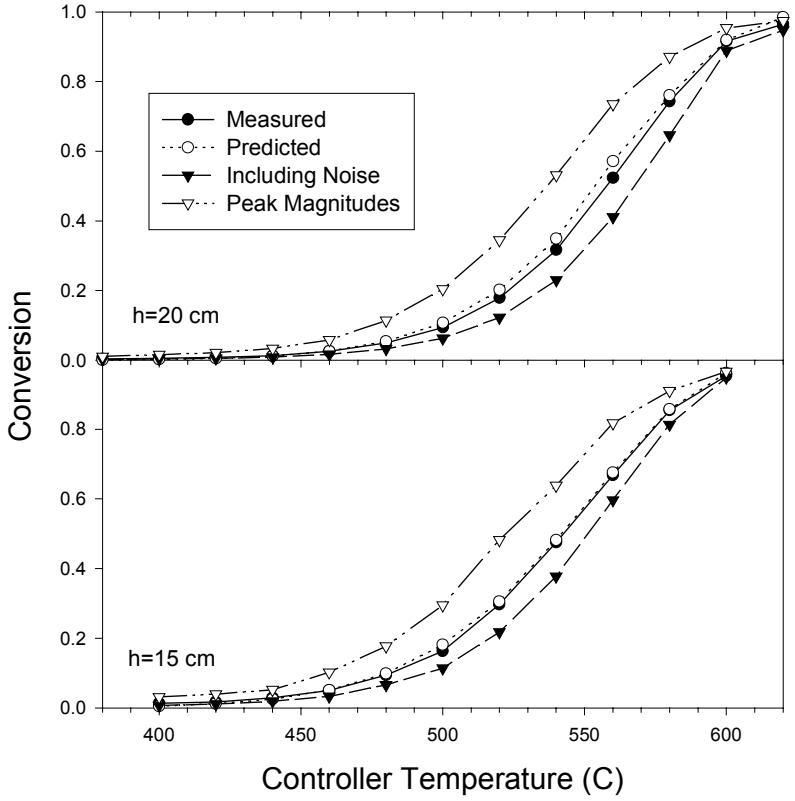

Figure 5: Allyl ethyl ether decomposition from two separate experiments

Particle Temperature

Changing from gas phase chemistry to solid phase particle chemistry further complicates the system. Particles are rigid, and denser than the gas phase molecules. Particle temperature is therefore expected to lag the gas temperature. Internal transport of heat within the particle should also contribute to the particle temperature lag. Radiation can increase or decrease particle temperature depending on the local radiative flux. Biomass pyrolysis is endothermic, and the heat of reaction can also contribute to a temperature lag. The dimensionless Biot number compares the ratio of the rates of convective and internal heat transport. Calculations showed that internal heat transfer is important for 100 μm particles, and could be important for smaller particles. The heat loss due to reaction depends strongly on the rate of reaction. The rate of reaction depends on the particle temperature, which may be a function of the heat loss due to reaction. Clearly, a more detailed analysis is needed to determine how small the particles need to be to maintain kinetic control of pyrolysis. Such a model can be derived from fundamental theories of heat transport. Three concentric solid zones were modeled to estimate the internal heat transport. Mass loss was modeled as the destruction of a concentric external layer of the particle. The energy conservation equations for a particle are as follows:

$$\dot{q}_n = \dot{q}_{conv} + \dot{q}_{reac} + \dot{q}_{cond} + \dot{q}_{zone\_transfer}$$

The term "q" is the energy [J] and the dot implies the first derivative with respect to time. The variable "n" represents the internal zone of the particle (i.e. 1,2,3). The convection term is:

$$\dot{q}_{conv} = Ah\left(T_{gas} - T_{solid}\right)$$

T is the temperature [K]. A is the surface area [m^2] of the particle and h is the convective heat transfer coefficient [J/m^2K], and is calculated from the following equation:

$$h = \frac{Nuk_f}{Dp}$$

Nu is the dimensionless Nusselt number, which has a value of 2.0 for small particles, k_f is the thermal conductivity of the gas [W/mK], and Dp is the particle diameter. The reaction term is defined by the following equation:

$$\dot{q}_{reac} = \Delta H_{reac} m_i \dot{x}$$

ΔH_{reac} is the heat of reaction [J/kg], m_i is the initial mass of the particle [kg], and x is the dimensionless conversion fraction. The conductive term comes from integrating Fourier's law in spherical dimensions, with the result being:

$$\dot{q}_{cond} = 4\pi k_p \left[\frac{\left(T_n - T_{n-1}\right)}{\left(1/r_n - 1/r_{n-1}\right)} - \frac{\left(T_{n+1} - T_n\right)}{\left(1/r_{n+1} - 1/r_n\right)} \right]$$

In this equation, r is the particle section radius [m], T is the temperature [K], and k_p is the thermal conductivity for the solid particle [W/mK]. Terms are only included when the subscript is 1,2, or 3. The final energy term $q_{zone\_transfer}$ is included because as the particle reacts, the dimension of the internal particle zones change. This term compensates for the mass energy lost as a result of the moving boundary:

$$\dot{q}_{zone\_transfer} = C_p \left(T_{n+1}\Delta V_{n+1\to n} - T_n \Delta V_{n\to n-1}\right)$$

C_p is the specific heat of the particle [J/kgK], T is temperature [K], and ΔV is the change in volume due to the particle reaction, and may be easily calculated from the radii of the particle zones. The radii of the particle zones are a direct function of the conversion, 'x'. Particle temperatures are initialized to the initial gas temperature, and particle zone energy is initialized to the sensible energy of the solid at that temperature. In this model, radiative heat transfer has been neglected. This a valid assumption, as the gas has been observed to rapidly assume the temperature of the nearby wall, and walls have been shown to be fairly opaque to thermal radiative transport. Radiative transport is a function of surface temperature differential, which is presumed to be quite low for smaller particles. Particle conversion, "x," is calculated from an Arrhenius rate equation:

$$\dot{x} = Ae^{-E/RT}$$

A is the pre-exponential factor [1/s], E is the activation energy [J/mol], R is the ideal gas constant [J/molK], and T is the reactant temperature [K]. In our model, T was the outer-most particle zone temperature, as mass loss was assumed to evolve from that zone. A time-temperature profile for a simulated particle of 20 μm diameter from the CFD simulations was used as input parameters. The model

stepped through discrete time steps to simulate the particle dynamics as they drop through the LEFR. The constants used to generate this plot are listed in Table 1. The parameters in Table 1 are for cellulose, with the exception of the thermal conductivity. The thermal conductivity was selected based on an average value of thermal conductivity for several types of wood. The rate constants are loosely based on the rate data from Milosavljevic and Suuberg (1995).

Table 1. Model constants assumed for the numerical study

Variable	Symbol	Value	Units
Arrhenius Pre-exponential Factor	A	4.0×10^{10}	1/s
Activation Energy	E	144.4	kJ/mol
Particle Specific Heat	C_p	2600	J/kgK
Particle Thermal Conductivity	k_p	0.11	W/mK
Heat of Reaction	ΔH_{reac}	-538	kJ/kg
Particle Density	ρ_p	1550	kg/m^3

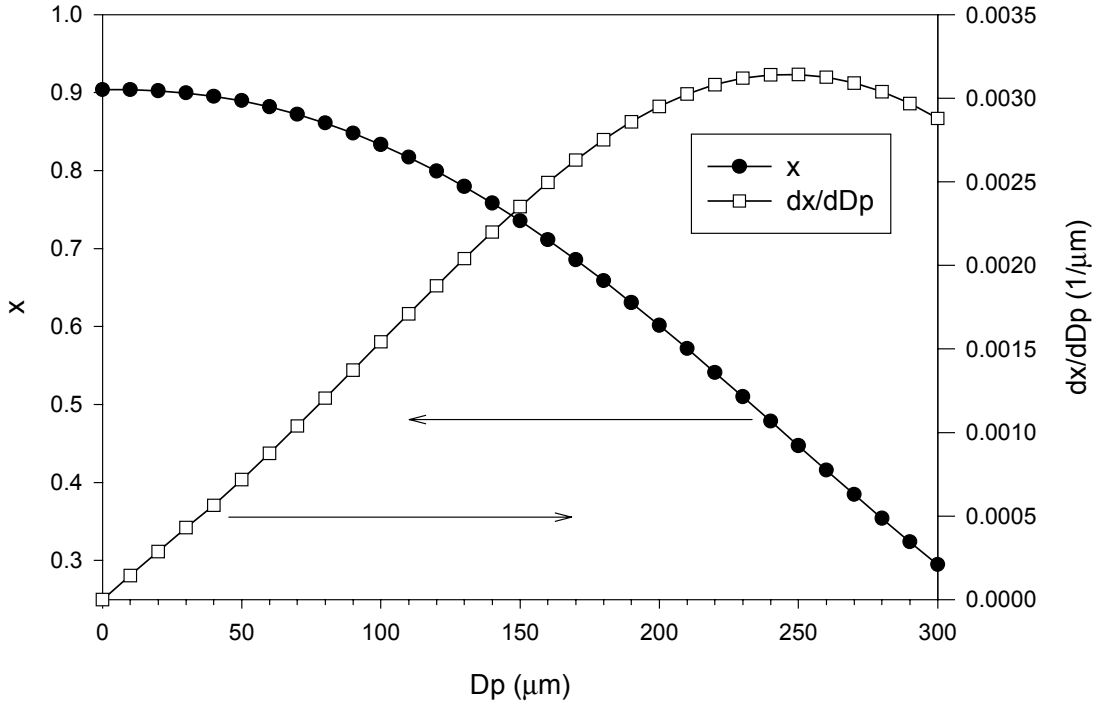

Figure 6: Predicted mass conversion of a cellulose particle as a function of particle diameter.

Figure 6 shows the mass conversion of cellulose in helium as a function of particle diameter, as well as an estimate of the change in conversion with respect to the particle size change (dx/dDp) as a function of the particle diameter. The time temperature profile was based on controller temperatures being set at 500 °C. As the particle size increases, the predicted conversion drops. This is attributed to particle-gas temperature lag, and is partly due to slower internal heat transport (further distance to heat) and partly to a higher heat demand (more mass to heat). Convection increases by the square of the particle size, and mass and volume increase by the cube of the particle size. The Dp=0 μm case is the ideal case with no heat transfer effects. The degree to which results vary from the ideal case indicates the degree to which

heat transfer rather than chemical kinetics influences the reaction dynamics. Values for dx/dDp for small particle diameters are fairly linear, and theoretically go to zero at Dp=0 μm. This allows results to be interpolated to Dp=0 μm. The model had difficulty predicting results for small particle diameters. Decreasing the step size can help circumvent this problem. With 12,000 steps, the model would still diverge for particles below about 14 μm. This is believed to be due to numeric precision issues from small energy values and cubing the particle diameter in meters. Since dx/dDp is linear in that regime, results for 30 μm particles and below were interpolated based on the observed trend, and values for x were calculated from the result. Results of this model demonstrate the importance of maintaining small particle sizes. For example, based on the model, we would expect results from particles 30 μm and smaller to be within about 0.8% of the ideal values. At 100 μm, an 8% error occurs due to particle size/heat transfer effects. This analysis may be a worst case scenario because of several factors. Rapid heating of biomass particles is known to result in fracturing of the particles. This would result in two particles, each half the mass of the initial particle, and would improve the kinetic limited assumption. Although difficult to quantify, radiation is thought to slightly improve this assumption as well. These results are sensitive to the values of many of the constants in Table 1. Changes in constant values may affect the data trends in Figure 6.

Particle Velocities

Particle velocity influences the time portion of the time-temperature profile. In a simplified case, all particles follow gas streamlines. Particle velocity lag occurs because the particle momentum does not allow it to follow gas streamlines. Larger particles are less likely to follow gas streamlines. This implies that there is an upper particle size limitation due to the gas/particle flow dynamics. Early gas/particle runs indicated that large agglomerates and larger particles tend to drop to the bottom of the reactor, while smaller particles exit out the sampling tube. This is undesirable, as the results rely on the assumption that all particles undergo a similar time-temperature profile. CFD runs can predict particle paths as a function of the gas flow-field and the particle size. Tests indicated that a biomass particle under about 50 μm and of typical density should follow the gas flow out the sampling tube. For particles above 100 μm, few will exit through the MBMS sample tube. It is desirable to have particles flow out the MBMS sample tube because as particles pyrolyze, mass loss occurs, changing the morphology and flow dynamics of the particles. Reducing particle lag through small initial particle size ensures that all particles take similar paths, regardless of prior mass loss.

Another concern in this regard is the influence initial particle release position has on the traced time-temperature profile. Although the bulk of the particles should flow in a relatively narrow region near the centerline of the reactor, not all will. Particles released horizontally and further away from the sample tube exit are expected to take longer to exit the system. This could skew the results of the experiment, as different particles would undergo different time-temperature histories. The analytical approach to this problem was to choose representative release positions and model decomposing particles released from those positions. Resulting variation should indicate the error induced by the variation in starting position. The assumption was that particles were evenly dispersed throughout the gas, and a Newtonian flow profile was assumed for the gas:

$$v_y(r) = v_o\left(1 - \frac{r^2}{R^2}\right)$$

In this equation, v_y is the y velocity, v_o is the velocity at the centerline, r is the radial position, and R is the radius of the cylindrical region. Integrating the flow profile over a differential area gives the volumetric flow rate in that area:

$$\dot{V} = \int_b^a v_y 2\pi r dr$$

This expression may be used to solve for the appropriate limits a and b that describe a given portion of the bulk flow. The resulting expression was solved to determine particle starting positions that represented the average initial bulk flow rate for particles in three equal-flow annular regions. Each annular region was divided into 4 separate regions, and Figure 7 illustrates the geometry of the sections used in this analysis.

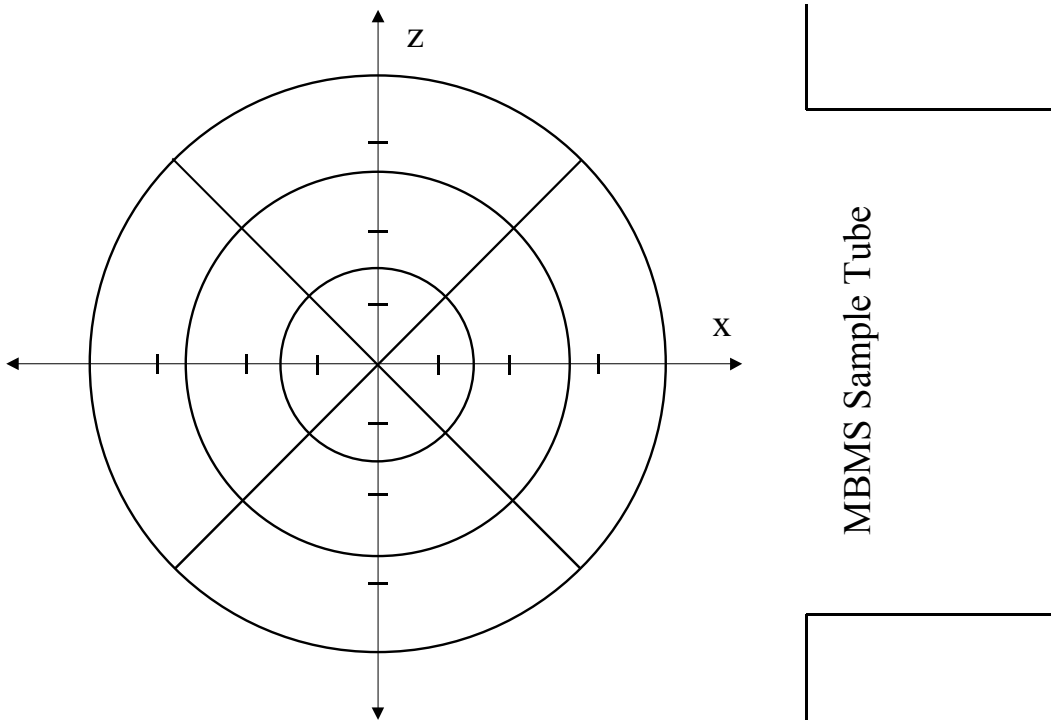

Figure 7: An illustration of the geometric sections assumed in the study of particle history variation due to starting location.

Figure 8 shows the results of a test based on a 400 °C temperature profile, h=20 cm, and 0.25 slm primary He flow, and 2 slm secondary He flow. This figure is representative of similar experiments at different flow rates. Conversion is lower for particles released closer to the centerline of the system. This is in part due to the higher velocity in that region and in part due to the gas temperature lag, which is slightly higher close to the centerline. Particles with starting positions further from the sample tube are expected to have higher conversion, as they must traverse a longer path to arrive at the exit. This trend is observed in the results in Figure 8. The average value crosses the trend of the x-line around 0.42 r/R. There is a strong correlation between the gas flow rates and the resulting simulated conversion in this study. Figure 9 shows a plot of the standard deviation of the predicted conversion versus the ratio of the primary to secondary gas flow rates. Secondary flow rates were varied between 1.5 slm and 3.0 slm, and primary flow rates were between 0.01 and 0.25 slm. Lower primary flow rates relative to the secondary gas flow results in improved variability. For gas flow rates of interest, this plot shows that there is a sharp increase in variability for primary to secondary flow ratios above about 0.08.

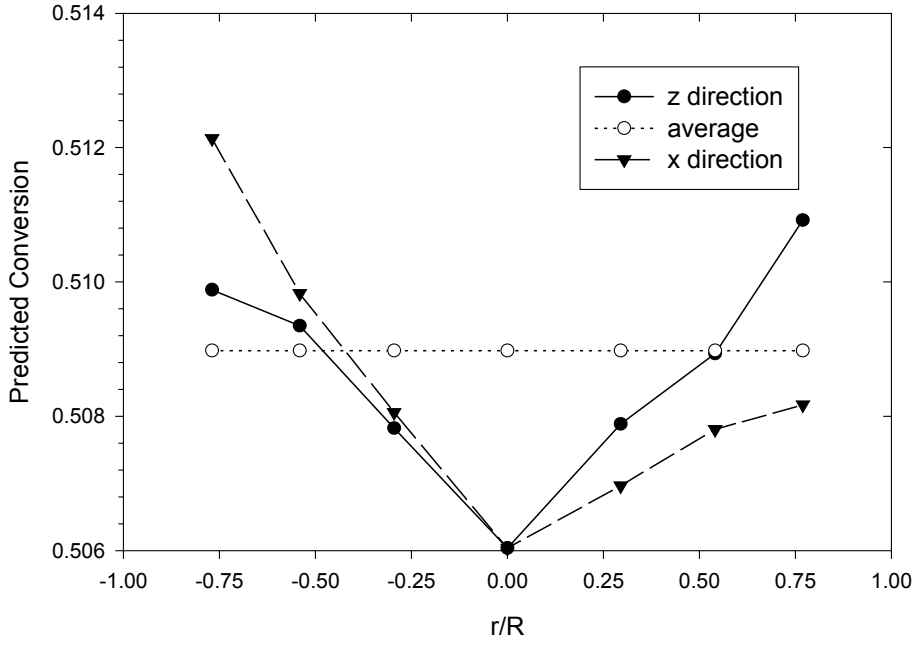

Figure 8: Predicted conversion for particles released in the feeding tube from various radial positions.

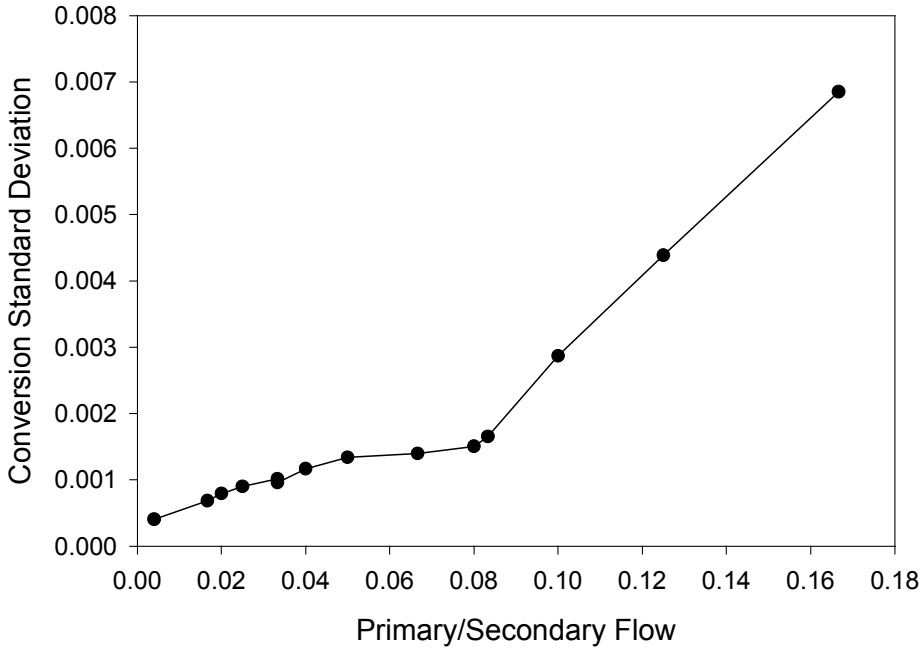

Figure 9: Standard deviation of predicted particle conversion for a bulk flow representative set at various gas flow rates.

Ideally, the corresponding points at ±z in Figure 8 should be equal because the system is symmetric about the x plane. They are not equal in some cases, and this is cause for concern. It may be attributed in part

to a non-symmetric grid, and in part to numerical diffusion. This implies that there is some degree of sensitivity to the grid formulation on the solution. Further grid refinement testing was performed, and did not improve the results, suggesting that the error is not due to grid being too coarse.

Several factors have not been taken into account with the model, which may influence particle velocities. Devolatilizing solids give off gas at a much lower density than the original solid. Large product gas increases relative to the bulk helium flow can increase the net velocity in the system. Keeping the bulk mass flow rate low relative to the mass flow rate of the gas can control this. Furthermore, a devolatilizing particle is changing in size, shape, and perhaps other properties such as density and thermal conductivity as it reacts. Thermophoretic particle diffusion and gas ejection momentum may also contribute to the distribution of particles and gas residence times in the system. Accurately accounting for these dynamic variations would be nearly impossible based on current knowledge, so these phenomena must be neglected.

A final observation that has made data reduction simpler in regard to particle velocities is that the velocity of the flow through the sampling tube is quite fast relative to other velocities in the system. This corresponds to a residence time of around 0.02 s. The temperature in this region is kept high, but is below the peak temperature of the reactor. This is to keep tars from condensing before the gas is sampled and quenched in the MBMS system. A strong temperature profile exists in this region, and has been measured with the reactor pulled back from the MBMS system. The temperature profile is thought to change as the two instruments are interfaced, making accurate temperature measurements difficult. Care was taken to input as accurate temperature information for this region as possible, until it was found that including this profile is superfluous because of the short gas and particle residence times. Modeling the wall temperature in this region at a constant value does not adversely affect the ultimate predictions, as minimal conversion has been observed in this region in all the modeling done thus far (fractions of a percent).

Particle Diffusion

Pyrolysis is not limited to the surface of a particle. A particle that undergoes uniform pyrolysis will form gases within the solid matrix, and will be unable to escape to the bulk gas region. Inter-particle diffusion is known to be important in many solid fuel pyrolysis studies. Gas diffusion can also limit surface and gas phase oxidation reactions, and alters the internal properties of a particle. These phenomena have not been addressed in detail, as diffusive limitations scale according to particle size. We assume that diffusion effects do not significantly influence the small particles used in our studies.

Feeding Solid Particles

A primary difficulty with most biomass related experiments is feeding the biomass into the reaction system. Our system will not be different. We have recently designed a new feeding system to feed low flow-rates of small diameter particles into a gas flow. Mass flow rates are typically on the order of 1 g/hr. An illustration of the particle feeder is in Figure 10. A syringe tube is connected to the housing of a variable speed (23-RPM maximum) motor to form an airtight seal. The motor shaft is connected to a brass tubing system. The brass tube has a hole near the bottom with brass agitating wires soldered above and below the hole. The useful range of hole sizes in the brass tube vary from 350 μm to 1 mm. A silicone rubber tube is fastened to a hole at the bottom of the syringe. Gas enters the syringe through this tube, and fluidizes the solid material, which exits down through the hole in the brass tube, and out the bottom of the syringe. The feed characteristics are a function of the gas flow rate, the size of the hole in the tube, and the speed of the motor. Some preliminary testing has been performed with cellulose particles varying in size from tens of microns to hundreds of microns. Generally, smaller particles feed better with smaller tube holes. Also, larger particles tend to feed better with lower gas flow rates. An increase in motor speed generally increases the feed rate. The dynamic range of feeding is difficult to control. We are also

considering additional feeder designs to give a broader range of feeding rates. Some information exists in the literature in regard to the design of such a feeding system [Burch et al., 1991; Geldart, 1973; Geldart and Abrahamsen, 1978; and Tang and Chen, 1999]

.

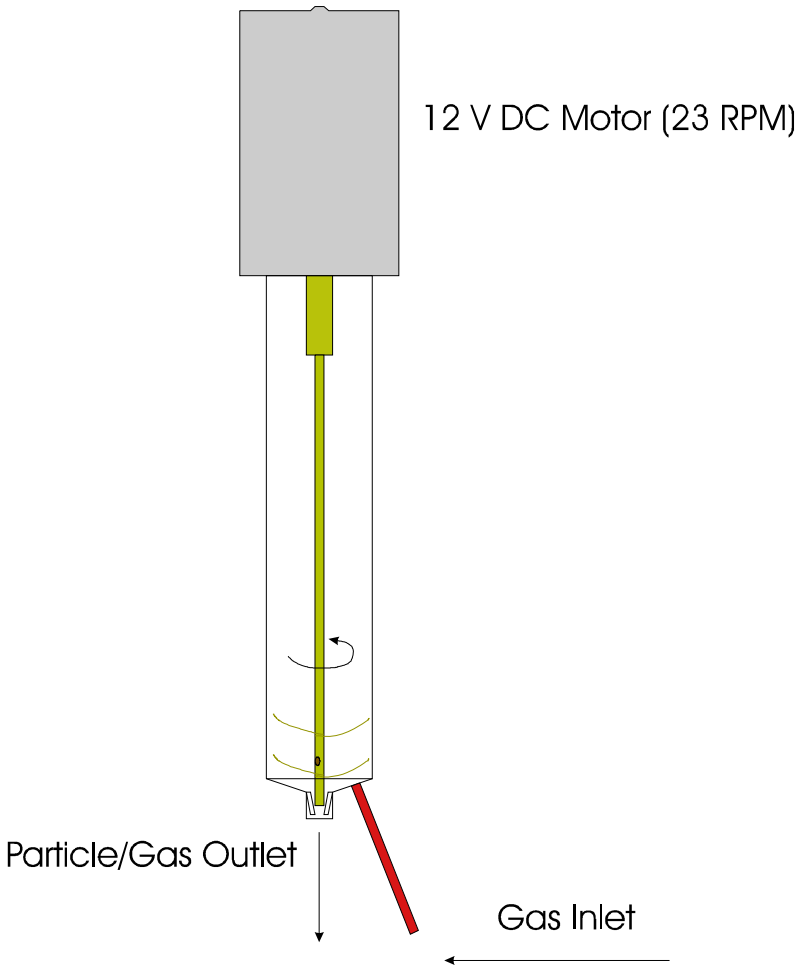

Figure 10: An illustration of the particle feeding system.

FUTURE WORK

1. Cellulose pyrolysis experiments are ongoing. Originally, cellulose was thought to be a good candidate for a calibration solid material, as there was considerable work in the literature on the rate of cellulose pyrolysis [Shafizadeh and Bradbury, 1979; Antal and Varhegyi, Diebold, 1994; and Milosavljevic and Suuberg, 1995]. After comparing several models, it was found that they all differed substantially. In some experiments, variations are attributed to heat and diffusive control regimes, variation in rate constants at different temperatures and heating rates, variations in cellulose sample quality, and unrepresentative global schemes. Most kinetic work has been done with TGA-type experiments at low heating rates. We hope to analyze cellulose pyrolysis at much higher heating rates, yet still in a kinetically controlled environment. These data will prove useful in determining an accurate model for cellulose pyrolysis, as there are no accurate data at such high heating rates.

2. Some further characterization is in order. Varying the size of cellulose particles fed into the reactor is a relatively simple experiment. We hope to see minimal variation in the decomposition rate at small particulate sizes, with variation increasing as the particle size increases. This will help confirm our assumptions with regard to thermal and diffusive transport control regimes.

3. Following the cellulose experiments, we will move on to biomass pyrolysis. The motivation for studying cellulose decomposition in the LEFR is to assess the gas product composition at various stages of solid fuel thermal decomposition. Kinetic studies have found that overlapping the rates of decomposition of the lignin, cellulose, and hemicellulose reasonably approximates the bulk rate of decomposition of the biomass. These data provide an attractive assumption, as decomposition rates are based on knowledge of the cellulose/lignin/hemicellulose composition. Several models already employ this assumption [Miller and Bellan, 1997 and Di Blasi and Russo, 1994]. We hope to analyze this assumption from a chemical products standpoint, as we should be able to detect chemical changes in decomposition with the MBMS system at different stages of pyrolysis.

SUMMARY

Much of the work that has gone into the design and characterization of the new LEFR indicates that this instrument is capable of accurately controlling particle pyrolysis. A combination of measurements and theoretical modeling contribute to the detailed understanding of the operating qualities of the reactor. There is excellent agreement between the model and the measurements with overlapping data between the two analytical techniques. Maintaining kinetic, rather than heat transport control is important to experimental value. Maintaining small (<50 μm) particle sizes is critical to both the control regime and to particle velocity lag in the reactor.

REFERENCES

Besseris, G.J., Kiefer, J.H., Zhang, Q., Walker, J., and Tsang, W., (1995). "The unimolecular dissociation of 3,4-dihydro-2H-pyran over a wide temperature range." *Int. J. of Chem. Kinetics* 27, 691-701.

Burch, T.E., Conway, R.B., and Chen, W.Y., (1991). "A practical pulverized coal feeder for bench-scale combustion requiring low feed rates," *Rev. Sci. Instrum. 62*, 480-483.

Di Blasi, C. and Russo, G., (1994). "Modeling of transport phenomena and kinetics of biomass pyrolysis." In A.V. Bridgwater, Ed. *Advances in Thermochemical Biomass Conversion*, vol. 2, pp. 906-921. Blackie Academic and Professional, New York.

Dayton, D.C., Belle-Oudry, D., and Nordin, A. (1999). "Effect of Coal Minerals on Chlorine and Alkali Metals Released during Biomass/Coal Cofiring." *Energy Fuels* 13(6) 1203-1211.

Dayton, D.C., French, R.J., and Milne, T.A. (1995). "The Direct Observation of Alkali Vapor Release during Biomass Combustion and Gasification 1. The Application of Molecular Beam/Mass Spectrometry to Switchgrass Combustion." *Energy Fuels, 9(5),* 855-865.

Dayton, D.C., Jenkins, B.M., Turn, S.Q., Bakker, R.R., Williams, R.B., Belle-Oudry, D., and Hill, L.M. (1999). "Release of Inorganic Constituents from Leached Biomass during Thermal Conversion" *Energy Fuels* 13(4) 860-870.

Dayton, D.C. and Milne, T.A. (1996). "Laboratory Measurements of Alkali Metal Containing Vapors Released During Biomass Combustion." Eds. Baxter, L. and DeSollar, R., *Application of Advanced Technologies to Ash-Related Problems in Boilers*, New York: Plenum Press, pp. 161-185.

Diebold, J.P., (1994). "A unified, global model for the pyrolysis of cellulose." *Biomass Bioenergy* 7, 75-85.

Egger, K.W. and Vitins, P., (1974). "The thermochemical kinetics of retro "ene" reactions of molecules with the general structure (allyl)XYH in the gas phase. IX. The thermal unimoleculaar decomposition of ethyallylether in the gas phase." *Int. J. of Chem. Kinetics* 6, 429-435.

Evans, R.J.and Milne, T.A. (1987a). "Molecular Characterization of the Pyrolysis of Biomass: I. Fundamentals." *Energy Fuels* 1, 123-137.

Evans, R.J. and Milne, T.A. (1987b). "Molecular Characterization of the Pyrolysis of Biomass: 2. Applications." *Energy Fuels* 1, 311-319.

Geldart, D., (1973). "Types of gas fluidization." *Powder Technology* 7, 285-292.

Geldart, D. and Abrahamsen, A.R., (1978). "Homogeneous fluidization of fine powders using various gases and pressures." *Powder Technology* 19, 133-136.

Fletcher, T.H., (1989). "Time-resolved particle temperature and mass loss measurements of a bituminous coal during devolatilization." *Combustion Flame* 78, 223-236.

Fletcher, T.H., (1993). "Swelling properties of coal chars during rapid pyrolysis and combustion." *Fuel* 72(11), 1485-1495.

Jamaluddin, A.S., Truelove, J.S., and Wall, T.F., (1986). "Devolatilization of bituminous coals at medium to high heating rates." *Combustion Flame* 63, 329-337.

Koufopanos, C.A., Maschio, G., and Lucchesi, A., (1989). "Kinetic modelling of the pyrolysis of biomass and biomass components." *Can. J. Chem. Eng.* 67, 75-84.

Koufopanos, C.A., Papayannakos, N., Maschio, G., and Lucchesi, A., (1991)." Modelling of the pyrolysis of biomass particles. Studies on kinetics, thermal and heat transfer effects." *Can. J. Chem. Eng.* 69, 907-915.

Lanzetta, M. and Di Blasi, C., (1998). "Pyrolysis kinetics of wheat and corn straw." *J. Anal. and Appl. Pyrol.* 44, 181-192.

Miller, R.S. and Bellan, J., (1997). "A generalized biomass pyrolysis model based on superimposed cellulose, hemicellulose and lignin kinetics." *Combust. Sci. Tech.* 126, 97-137.

Milosavljevic, I. and Suuberg, E.M., (1995). "Cellulose thermal decomposition kinetics: Global mass loss kinetics." *Ind. Eng. Chem. Res.* 34, 1081-1091.

Neusser, H.J. and Krause, H., (1994). "Decay energetics of molecular clusters studied by multiphoton mass spectrometry and pulsed field threshold ionization." *Int. J. of Mass Spectr. and Ion Proc.* 131, 211-232.

Orfao, J.J.M., Antunes, F.J.A., and Figueiredo, J.L., (1999). "Pyrolysis kinetics of lignocellulosic materials-three independent reactions model." *Fuel* 78, 349-358.

Pollard, R. (1997). "Influence of the cooling section on vapor-phase pyrolysis in laminar-flow reactors." *J. Anal. and Appl. Pyrol.* 39, 145-160.

Shafizadeh, F. and Bradbury, A.G.W., (1979). "Thermal degradation of cellulose in air and nitrogen at low temperatures." *J. of Appl. Polymer Sci.* 23, 1431-1442.

Tang, L. and Chen, W.Y., (1999). "Improvements on a particle feeder for experiments requiring low feed rates." *Rev. Sci. Instrum.* 70, 7, 3143-3144.

Wagenaar, B.M. and Van den Heuvel, E.J.M.T., (1997). "Co-combustion of misanthus in a pulverised coal combustor: experiments in a droptube furnace." *Biomass Bioenergy* 12(3) 185-197.

Ward, S.M. and Braslaw, J., (1985). "Experimental weight loss kinetics of wood pyrolysis under vacuum." *Combustion Flame* 61, 261-269

Westerhout, R.W.J., Kuipers, J.A.M., and Van Swaaij, W.P.M., (1996). "Development, modelling and evaluation of a (laminar) entrained flow reactor for the determination of the pyrolysis kinetics of polymers." *Chem. Eng. Sci.* 51(10), 2221-2230.